Evaluation of energy efficiency, visualized energy, and production of environmental pollutants of a solar flat plate collector containing hybrid nanofluid

Jawed Mustafa [a,*], Saeed Alqaed [a], Mohsen Sharifpur [b,c,*]

[a] Mechanical Engineering Department, College of Engineering, Najran University, P.O. Box (1988), Najran 61441, Saudi Arabia
[b] Department of Mechanical and Aeronautical Engineering, University of Pretoria, South Africa
[c] Department of Medical Research, China Medical University Hospital, China Medical University, Taichung, Taiwan

ARTICLE INFO

Keywords:
Flat plate solar collector
Energy efficiency
Visualized energy
Environmental analysis
Pollutant production

ABSTRACT

Energy efficiency, visualized energy, and production of environmental pollutants of a solar flat plate collector containing water/copper–aluminum hybrid nanofluid are evaluated. The results are compared with water/aluminum oxide nanofluid and water. The Reynolds number (Re) for the investigation is between 700 and 2300, and the nanoparticles volume fraction is 0.1%. A developed model in the engineering equations solver is used to solve the governing equations. The outputs show that the most suitable collector operating fluid is the hybrid nanofluid. Collector energy efficiency employing hybrid nanofluid is more than other operating fluids, and its maximum increment applying mono and hybrid nanofluids relative to water is 3.86 and 4.23 %, respectively. The criterion evaluation performance of the collector in the presence of hybrid nanofluid is larger than mono-nanofluid of aluminum oxide–water. Environmental analysis of the collector shows that the productions of sulfur oxides, carbon dioxide, and nitrogen oxides in a solar flat plate collector are maximum and minimum for water and hybrid nanofluid, respectively. In the case of hybrid nanofluid, the rate of production reduction of carbon dioxide, sulfur oxides and nitrogen oxides are respectively 29.15 kg, 0.0149 kg and 0.0255 kg compared to water. However, these amounts are 26.64 kg, 0.0136 kg and 0.0233 kg for mono nanofluids, respectively.

Introduction

Because of the challenges of fossil fuels in supplying human energy, including global warming and environmental pollution, solar energy is the most promising solution to overcome these challenges [1–3]. As everyone knows, environmental pollution and its effects on climate and community life have led researchers to conduct extensive research on the environment and how to keep it healthy [4–6]. Today, solar energy is a good help to solve human crises, which includes various uses such as electricity supply, fresh water, heating, cooling, etc [7–9]. The most common use of solar energy for heat supply is solar flat plate collectors. This type of collector is known as one of the most efficient and unpolluted heating systems [10]. The main disadvantage of this type of collector is its low efficiency. With the advancement of nanotechnology and the use of nanoparticles in various industries, many researchers have used them in their research [72–74]. Significantly, the utilization of nanofluids instead of conventional heat transfer fluids such as ethylene glycol or water can improve their performance [13–15]. Accordingly, this is an important method of studying solar collectors in the last decade [16,17]. Since the nanoparticles' thermal conductivity is higher than the base fluid, the improvement of the overall performance of the collector is enhanced [18,19].

New generations of refrigerants that have been introduced in the last decade are hybrid nanofluids (HYBNs). They are a good choice as a working fluid in solar collectors due to their ability to absorb solar radiation at wavelengths of 200 to 1100 nm [20,21]. Also, most studies in flat plate collectors using HYBNs have reported that the thermal efficiency of the collector when HYBN is employed is higher than mono nanofluids and base fluids [22]. Farajzadeh et al. [23] tested the effect of aluminum oxide/titanium dioxide-water HYBNs and aluminum oxide–water and titanium dioxide-water mono nanofluids on the performance of a solar flat plate collector (FPSC) numerically and

* Corresponding authors at: Mechanical Engineering Department, College of Engineering, Najran University, Najran, Saudi Arabia (J. mustafa). Department of Mechanical and Aeronautical Engineering, University of Pretoria, South Africa (M. Sharifpur).
E-mail addresses: jmmustafa@nu.edu.sa (J. Mustafa), mohsen.sharifpur@up.ac.za (M. Sharifpur).

experimentally. The findings indicated that comparing to base fluid and mono nanofluids, the HYBN has a better operation. Accordingly, the rate of increase of collector thermal efficiency using HYBN is equal to 26%, 19%, and 21% compared to water, aluminum oxide–water, and titanium dioxide-water, respectively. The evaluation of the performance of a FPSC from energy and exergy perspectives using magnesium oxide HYBNs/ MWCNTs-water and copper oxide/MWCNTs-water and magnesium oxide–water, copper oxide–water, and multi-walled carbon–-water was done by Verma et al. [24]. Their experimental findings indicated that the maximum thermal efficiency and collector exergy efficiency are obtained when MWCNTs-water mono nanofluid is employed as the operating fluid under different conditions. This includes solar radiation intensity, volume fraction, rate of mass flow, and inlet temperature. Magnesium oxide/MWCNTs-water and copper oxide/MWCNTs have second and third thermal efficiency values. Hussein et al. [25] combined CF-MWCNTs, CF-GNPs, and h-BN nanoparticles in water as the based fluid to prepare a new HYBN and evaluate the performance of a FPSC experimentally. They found that the thermal efficiency of collector using HYBN is better than the base fluid. The maximum increment in thermal efficiency of the collector using HYBN was reported to be 20% compared to water. Exergy and energy analysis of a FPSC was performed utilizing aluminum oxide/iron-water HYBN by Okonkwo et al. [26]. Their study showed that the collector's performance when aluminum oxide–water mono nanofluid is employed is better than HYBN. Accordingly, an increment in the thermal efficiency and coefficient of heat transfer of aluminum oxide–water mono nanofluid is equal to 2.16 and 72% compared to the base fluid, respectively. For aluminum oxide/iron-water HYBN they were equal to 1.79 and 56, respectively. On the other hand, they showed that the collector's efficiency of exergy applying aluminum-water mono nanofluid and HYBN is 5.7% and 6.9% higher than water, respectively. The influence of copper/copper oxide–water HYBN on exergy and energy efficiencies of a FPSC was studied by JA and Kumar [27]. Their findings indicated that the collector's efficiency of exergy and energy when HYBN is employed is higher than other operating fluids. They reported that the increment in the collector's thermal efficiency by applying HYBN, copper–water, and copper oxide–water mono nanofluids is 2.175, 0.93, and 1.05%, respectively, compared to the base fluid. The increase was equal to 2.59, 2.32, and 2.18% for the exergy efficiency, respectively. In an experimental study, Wole-Osho et al. [28] evaluated the performance of a FPSC using aluminum oxide/zinc oxide–water HYBN. They used different volume ratios of aluminum oxide to zinc oxide equal to 50:50, 66.66:34.34, and 33.34–66.66% and showed that the rate of increase of collector thermal efficiency using aluminum oxide/zinc oxide HYBN is equal to 7, 5, and 4.5% compared to the base fluid, respectively. The rate of collector exergy efficiency increase was equal to 6, 7.5, and 9%, respectively. Sundar et al. [29] tested the performance of a FPSC experimentally applying iron oxide–water nanofluid and reported that the maximum increase in the collector's thermal efficiency using nanofluid is about 27% compared to the base fluid. Tahat and Benim [30] evaluated the performance of a FPSC experimentally employing a combination of aluminum oxide and copper oxide nanoparticles in a mixture of water and ethylene glycol. They reported that the collector's thermal efficiency applying a HYBN is 45% higher than that when the fluid is water. Sundar et al. [31] assessed the influence of nanodiamond/cobalt-water HYBN on FPSCs and indicated that for the volume fraction of 0.15%, the collector's thermal efficiency used HYBN is 20% more than that employed the base fluid.

Due to the environmental pollutants such as sulfur oxides, carbon dioxide, and nitrogen oxides for the life of human societies, their reduction is of particular importance in heat transfer systems. In FPSCs, the energy visualization approach is used to study the production of these environmental pollutants. Faizal et al. [32] examined the production of sulfur oxides, carbon dioxide, and nitrogen oxides for a FPSC applying copper oxide–water, aluminum oxide–water, titanium dioxide-water, and silicon-water dioxide nanofluids. Their study demonstrated that water is the most polluting fluid based on the production of pollutants. Stalin et al. [33] used a cerium oxide–water nanofluid with various volume fractions to perform an environmental analysis of a FPSC. They reported that the minimum amounts of sulfur oxides, carbon dioxide, and nitrogen oxides occur when the operating fluid of the cerium-water oxide nanofluid collector has a volume fraction of 0.05%, and the maximum amount of pollutants is related to the water. In another study, Faizal et al. [34] conducted an environmental analysis of a FPSC employing silicon dioxide-water nanofluid. The results revealed that silicon dioxide-water nanofluid is a more suitable working fluid than water due to the production of fewer pollutants.

Previous researches have shown that the use of metal nanoparticles such as copper in water-based fluid enhances the thermal efficiency of the FPSC by 24% [35]. Moreover, one of the most widely used nanoparticles is aluminum oxide and the cheapest nanoparticles used in solar collectors studies [36–41]. Since aluminum oxide/copper nanocomposite has been synthesized in the laboratory and the suspension of particles of this nanocomposite in water has very good stability and also has better thermophysical properties than water [42–47,75,76], it can be a good option for FPSCs. Moreover, less attention has been paid to the environmental analysis of FPSCs employing HYBNs. Hence, in the present study, the influence of aluminum oxide/copper–water HYBN on the performance of a flat plate collector is compared with aluminum oxide–water mono nanofluid and base fluid. The nanoparticles volume fraction is 0.1%, and the Re is considered in the range of 700 to 2300. Also, the fluid flow regime in the collector is considered laminar. A model developed in the engineering equations solver is employed to solve the nonlinear governing equations. In this study, the effect of different fluids and nanofluids on the production of carbon dioxide, sulfur oxides and nitrogen oxides of a flat solar collector has been investigated, which has been less considered so far. Hybrid nanofluids have recently received more attention due to their greater advantages over conventional nanofluids. Improvements in the thermophysical properties and the thermal conductivity of hybrid nanofluids have been considered in this study.

Materials and methods

This study uses a FPSC and a plate-and-tube model to analyze the aluminum oxide/copper–water HYBN. The tubes carrying the working fluid are in the middle of the plate. Fig. 1 shows a configuration of the FPSC studied in the present work. The absorber plate'S area is 2 m^2 and the number of pipes is 6.

Table 1 presents the structural specifications and optical properties of the collector. The number of glass covers is assumed to be 1, the collector angle with respect to the horizon is equal to 45°, and the outer diameter of the pipes is assumed to be 11 mm. Also, the working fluid is

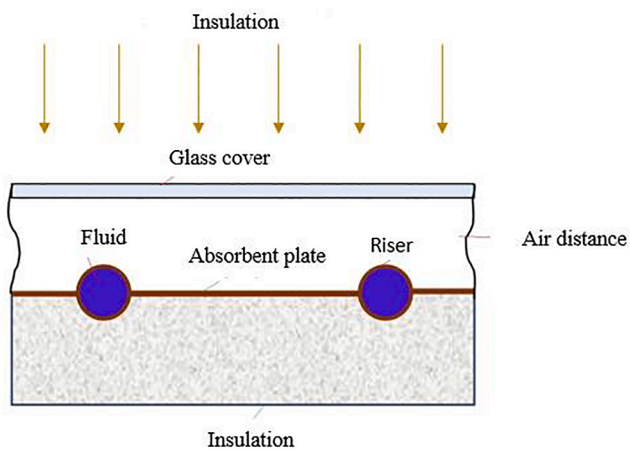

Fig. 1. A view of the FPSC.

Table 1
Dimensional specifications and optical properties of the studied FPSC [48].

Parameter	Value	Unit
Collector absorber plate area	2	(m^2)
Length	2	(m)
Width	1	(m)
Collector height	80	(mm)
Pipe inner diameter	10	(mm)
Distance from the center to the center of the pipes	150	(mm)
Absorbent plate thickness	0.5	(mm)
Absorbent plate thermal conductivity	385	(W/m K)
Absorbent plate absorption coefficient	0.92	–
Transparent coefficient of the glass cover	0.84	–
Absorbent plate emissivity	0.05	–
Emissivity of the glass cover	0.85	–
Collector back insulation thickness	50	(mm)
Insulation thickness of collector sides	25	(mm)
Thermal conductivity of insulation	0.025	(W/m K)

assumed as incompressible and Newtonian, and the fluid flow regime is considered laminar.

Mathematical modeling

Solar radiation moves through the FPSC glass cover and collides with the absorber plate and the tubes involved heat transfer fluid. A part of the absorbed radiation is transferred to the working fluid by the absorber plate and tubes, and the other part is wasted. Therefore, the amount of useful energy entering the working fluid or the useful energy leaving the collector is obtained according to the below equation [49]:

$$Q_u = A_c[S - U_L(T_{pm} - T_a)] \quad (1)$$

where A_c, S, U_L, T_{pm}, and T_a is the area of the absorber plate (m^2), the absorbed solar energy (W/m^2), the total coefficient of heat loss (W/m^2K), the absorber plate's average temperature in K and the ambient temperature in K, respectively.

As shown in Fig. 1, heat loss occurs due to the three paths of the top part of the absorber plate (air gap and glass cover), the bottom part, and the sides. Therefore, the total coefficient of heat loss contains of three parts: the top coefficient of heat loss U_t, the bottom one U_b, and the sides one U_e, and is defined as Eq. (2) [49]:

$$U_L = U_t + U_b + U_e \quad (2)$$

Insulation layers are used on the bottom and sides of the collector to decrease heat loss. The heat loss coefficient is calculated according to the following equation [50]:

$$U_b = \left(\frac{L_b}{k_b} + \frac{1}{h_{b,a}}\right)^{-1} \quad (3)$$

where L_b is the insulation thickness at the bottom of the collector (m), k_b is the thermal conductivity of the insulation (W/mK), and $h_{b,a}$ is the convection heat transfer coefficient at the bottom (W/m^2K).

The lateral coefficient of heat loss is calculated according to the below equation [50]:

$$U_e = \left(\frac{L_e}{k_b} + \frac{1}{h_{e,a}}\right)^{-1}\frac{A_e}{A_c} \quad (4)$$

where L_e is the insulation thickness at the collector side (m), $h_{e,a}$ is convection coefficient of heat transfer at the side (W/m^2K) and A_e are the collector side area (m^2). In this paper, the values of $h_{e,a}$ and $h_{b,a}$ are equal to 5 W/m^2K.

In this paper, the classical fin analysis method is used to calculate the performance of the FPSC. In fact, the absorber plate of the collector acts as a fin and transfers the absorbed heat to the operating fluid. A part of the heat enters the working fluid through fluid-carrying tubes exposed to sunlight. The classical fin analysis technique is presented in detail in references [49] and [50]. Here, only the required relationships are presented.

The absorber plate's average temperature is defined as follows [49]:

$$T_{pm} = T_i + \left(\frac{Q_u}{A_c U_L F_R}\right)(1 - F_R) \quad (5)$$

where the inlet temperature (T_i), which in this paper is constant and equal to 305.15 K. F_R is the heat transfer factor of collector that is calculated based on the following equation [49]:

$$F_R = \frac{\dot{m}C_{pf}}{A_c U_L}\left[1 - \exp\left(\frac{-A_c U_L F'}{\dot{m}C_{pf}}\right)\right] \quad (6)$$

where $\dot{m}$, C_{pf}, and F' is the mass flow rate (kg/s), specific heat of the working fluid and the collector efficiency coefficient.

The coefficient of the collector efficiency is obtained according to the following equation [49]:

$$F' = \left(W\left[\frac{1}{(D + (W - D)F)} + \frac{U_L}{\pi D_i h_{fi}}\right]\right)^{-1} \quad (7)$$

where W is the distance from the center to the center of the fluid-carrying tubes, D is tube's outer diameter, F indicates the standard fin efficiency, and h_{fi} is the convection coefficient of heat transfer of the working fluid.

The standard fin efficiency is defined as follows [49]:

$$F = \frac{\tanh(m(W - D)/2)}{m(W - D)/2} \quad (8)$$

where k_p represents the absorber plate's thermal conductivity and δ_p is the thickness of the absorber plate.

The convection coefficient of heat transfer of the working fluid is calculated as follows [49]:

$$h_{fi} = \frac{Nuk_{bf}}{D_i} \quad (9)$$

In Eq. (9), Nu represents the working fluid's Nusselt number and k_{bf} is the base fluid's thermal conductivity.

FPSC energy efficiency is the ratio of useful output energy from the collector to the amount of solar radiant energy available at the collector inlet is defined as follows [49]:

$$\eta = \frac{Q_u}{A_c G_T} \quad (10)$$

The pressure drop in the flat plate collector with an inclination angle of β is calculated as follows [51].

$$\Delta P = \rho_f g(L\sin\beta + h_L) \quad (11)$$

Comparison of the pumping power of base fluid and HYBN can be important. The pumping power relationship is defined as follows [52]:

$$W_p = \dot{m}\frac{\Delta p}{\rho_f} \quad (12)$$

In this paper, performance evaluation criteria (PEC) is used at constant pumping power and constant pressure drop to determine the utilization of mono nanofluid and HYBN.

The PEC at constant pumping power is expressed as follows [53]:

$$PEC\ I = \left(\frac{Nu_{nf}}{Nu_{bf}}\right)\left(\frac{f_{nf}}{f_{bf}}\right)^{-\frac{1}{3}} \quad (13)$$

The PEC at constant pressure drop is as follows [54]:

$$\text{PEC II} = \left(\frac{Nu_{nf}}{Nu_{bf}}\right)\left(\frac{f_{nf}}{f_{bf}}\right)^{-\frac{1}{2}} \quad (14)$$

Thermophysical properties of the base fluid and nanofluid

The base fluid's thermophysical properties are assumed to be a function of temperature and are calculated at the fluid's average temperature. These properties can be extracted from [55] and [56] (see the Appendix).

The thermophysical properties of Aluminum/Copper-Water HYBN and Aluminum monoxide-water nanofluid, including thermal conductivity and dynamic viscosity extracted based on experimental results [44]. These properties have been used in several other studies related to heat transfer [57,58].

Table 2 presents the dynamic viscosity and thermal conductivity of aluminum oxide/copper–water HYBN and aluminum oxide–water mono nanofluid for a volume fraction of 0.1%.

To determine the density and specific heat of HYBN and mono nanofluid, the thermophysical properties of nanoparticles are used based on Table 3.

The relationship between the volume fraction of nanoparticles is expressed as follows:

$$\phi = \phi_1 + \phi_2 \quad (15)$$

where ϕ_1 and ϕ_2 are the volume fraction of aluminum oxide and copper nanoparticles, respectively. ϕ is the nanocomposite's volume fraction. In this article, ϕ_1 and ϕ_2 equal to 0.0038% and 0.0962%, respectively.

The density and specific heat and density of the nanocomposite and nanofluid are determined based on the (22-a) to (22-d) equations [61,62].

Validation

To verify the present results, the results of the study of Jafarkazemi and Ahmadifard [63] are used. Jafarkazemi and Ahmadi-Fard [63] calculated the performance of a FPSC from exergy and energy perspectives theoretically and experimentally. They estimated the energy efficiency of the FPSC at various inlet temperatures. Fig. 2 compares the energy efficiency of the present study with those reported by Jafarkazemi and Ahmadifard [63] according to the heat loss parameter. The average error between the present work's results and the study of Jafarkazemi and Ahmadifard [63] is equal to 3.16%, indicating that the model developed in this study has high accuracy.

Results

To study the performance of the FPSC, different thermal and hydrodynamic parameters are analyzed using aluminum oxide/copper–-water HYBN and aluminum oxide–water mono nanofluid. These parameters include energy efficiency, total heat loss coefficient, absorber plate temperature, Nusselt number, friction coefficient, pressure drop, and pumping power. In addition, the comparison of PEC at constant pumping power (PEC I) and constant pressure drop (PEC II) for nanofluids is also performed. The nanoparticles' volume fraction of is constant and equal to 0.1%, the fluid inlet temperature is equal to 32 °C, and the Re is considered in the range between 700 and 2300. Also, impact radiation on the collector is assumed to be equal to 900 W/m^{2}K, wind speed equal to 7 m/s, and ambient and sky temperatures are 20 °C [48].

Table 2
Thermophysical properties of HYBN and mono nanofluid [44].

Nanofluid	k_{nf} (W.m-1 K^{-1})	μ_{nf} (Pa.s)
Aluminum oxide/copper–water	0.619982	0.614055
Aluminum oxide–water	0.000972	0.0009041

Table 3
Thermophysical properties of nanoparticles used in this study [59,60].

Nanoparticle	ρ (kg.m^{-3})	c_p (J.kg^{-1}K^{-1})
Al_2O_3	3970	765
Cu	8933	385

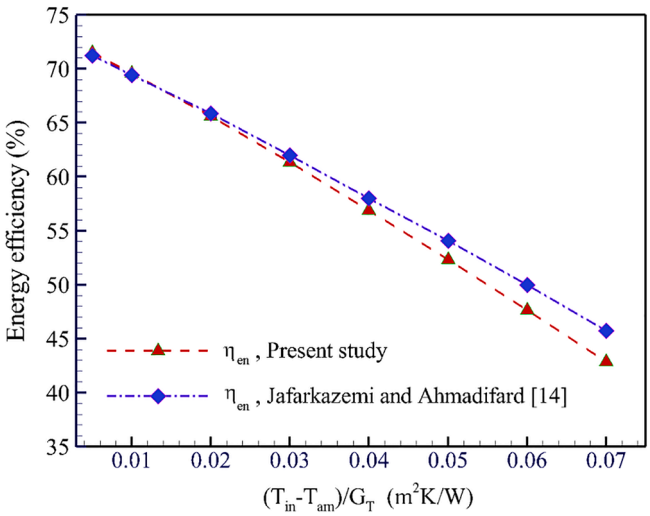

Fig. 2. The energy efficiency obtained from the present study and reported by Jafarkazemi and Ahmadifard [63].

Fig. 3 shows the energy efficiency of the FPSC for various working fluids in terms of Re. Fig. 3 demonstrates the higher energy efficiency of the collector by employing the HYBN and mono nanofluids instead of the base fluid. Also, the collector's efficiency of energy using HYBN as the working fluid is higher than mono nanofluid. At Re of 700, the rate of increase of collector energy efficiency using aluminum oxide–water mono nanofluid is equal to 3.86% compared to the base fluid, and for aluminum oxide/copper–water HYBN is equal to 4.23%. As the Re enhances, the collector energy efficiency for all working fluids is intensified. However, the increase in collector energy efficiency for nanofluids is slightly less than for water. At Re of 2300, the rate of increase of collector energy efficiency for HYBN and mono nanofluid is equal to 3.29 and 3.16%, respectively, relative to water. On the other hand,

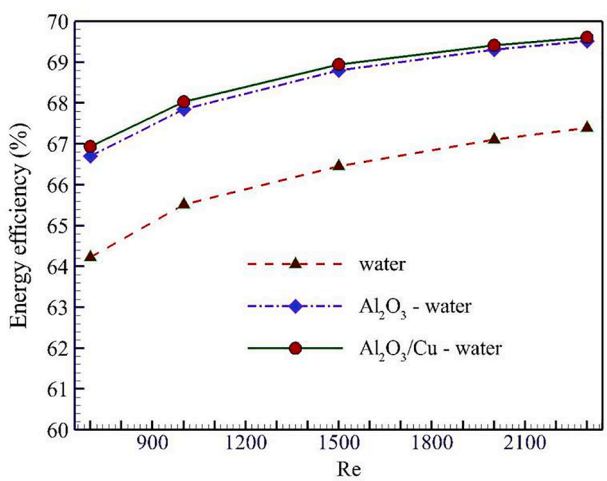

Fig. 3. The energy efficiency of base fluid, mono nanofluid, and HYBN in terms of Re.

according to Fig. 3, it can be seen that the collector energy efficiency diagrams become asymptotic by increasing the Re. By enhancing the Re from 700 to 2000, the increase in collector energy efficiency for water, mono nanofluid, and HYBN is equal to 2.02, 1.72, and 1.63%, respectively. Besides, by enhancing the Re from 2000 to 2300, the enhancement in collector energy efficiency for water, mono nanofluid, and HYBN is equal to 0.42, 0.3, and 0.27%, respectively.

According to Fig. 3, the collector's energy efficiency employing HYBNs is slightly more than aluminum monoxide-water nanofluid. Compared to mono nanofluid, the increase of collector energy efficiency using HYBN at Reynolds numbers of 700 and 2300 is 0.36% and about 0.13%, respectively.

Due to the constant amount of radiation flux and radiation properties of the collector, the amount of energy absorbed by the collector is constant. Therefore, an increment or reduction of energy efficiency depends on changes in the amount of useful energy output from the collector (Q_u). The amount of useful energy is also affected by the amount of heat loss. For this reason, it is important to investigate the amount of heat loss. According to Eq. 1, the amount of heat loss depends on the coefficient of total heat loss (U_L) and the average temperature of the absorber plate (T_{pm}). Therefore, these two parameters are examined below.

The total heat loss coefficient following Eq. (2) contains of a top, bottom, and side coefficients of heat loss. In Figs. 4a and 4b, the top coefficient of heat loss and Fig. 5, the total heat loss coefficient of the FPSC for the base fluid and nanofluid, are plotted at different Reynolds numbers. Calculations show that about 83% of U_L belongs to U_t, and only 17% belongs to the bottom and sides coefficients of the heat loss for all working fluids.

As shown in Fig. 4, the collector's coefficients of top and total heat loss in the presence of the HYBN is less than the mono nanofluid and water. This is because of the higher heat transfer coefficient of the HYBN compared to other working fluids. Furthermore, it is concluded that a lower total heat loss coefficient for HYBN leads to higher collector efficiency of energy than base fluid and mono nanofluid. By enhancing the Re, the total heat loss coefficient for all working fluids decreases due to an increasing trend of convection heat transfer coefficient with the Re.

One of the most influential parameters in collector performance in terms of energy and lifetime is the absorber plate's temperature. Fig. 5a shows the average temperature of the flat plate collector absorber plate for HYBN, mono nanofluid, and water in terms of Re. For a given Re, the temperature of the absorber plate with HYBN is lower than that of the mono nanofluid and base fluid. For example, at Re of 700, the rate of decrease of absorber plate temperature for HYBN and mono nanofluid is

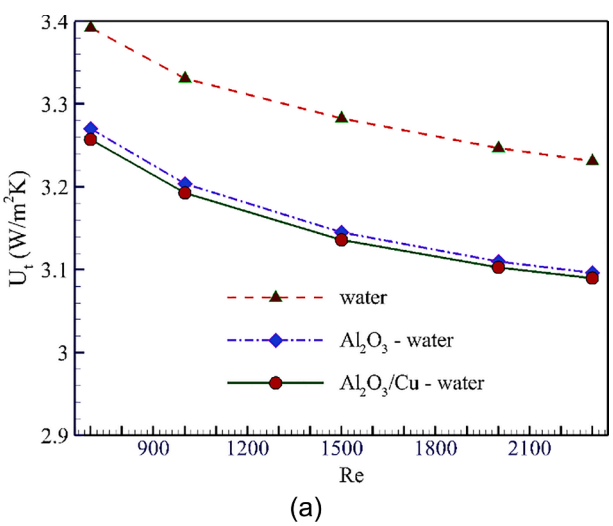

Fig. 4a. Top heat loss coefficient for different working fluids in terms of Re.

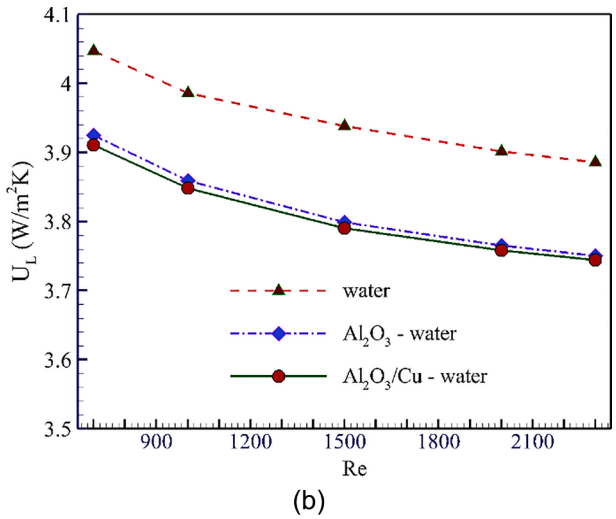

Fig. 4b. Total heat loss coefficient for different working fluids in terms of Re.

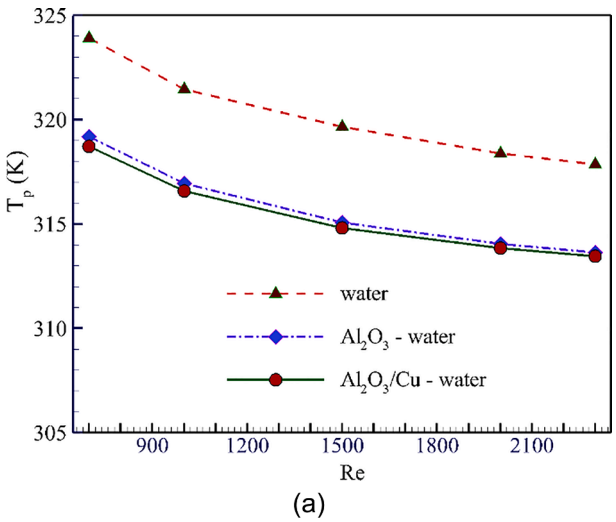

Fig. 5a. Absorber plate temperature for various working fluids versus Re.

equal to 5.19 and 4.72 K, respectively, relative to water. At Re of 2300, it is equal to 4.4 and 4.22 K, respectively.

According to Fig. 4, the trend of changes in the diagrams of the two figures is similar. The higher the absorber plate's temperature, the higher total heat loss coefficient, and vice versa. On the other hand, based on Fig. 3, the trend of energy efficiency is opposite to the coefficient of total heat loss and the absorber plate's average temperature. Therefore, increasing or decreasing the collector energy efficiency depends on the total heat loss coefficient and the absorber plate's average temperature.

An increment in the heat transfer factor decreases the absorber plate's temperature and consequently enhances the energy efficiency of the collector. Fig. 5b shows the collector heat transfer factor for water and nanofluids in terms of Re. The collector heat transfer factor has the maximum and minimum values for HYBN and water, respectively. Table 4 shows the amounts of F_RU_L, $F_R(\tau\alpha)$, and η_{en} for the FPSC for different working fluids at Re of 2000. Higher $F_R(\tau\alpha)$ and a lower F_RU_L increase the energy efficiency and indicate that the working fluid is more suitable for the flat plate collector. According to Table 4, the maximum amount of F_R $(\tau\alpha)$ and the minimum amount of F_RU_L are related to the aluminum oxide/copper–water HYBN, followed by the aluminum oxide–water mono nanofluid, and the base fluid. Therefore,

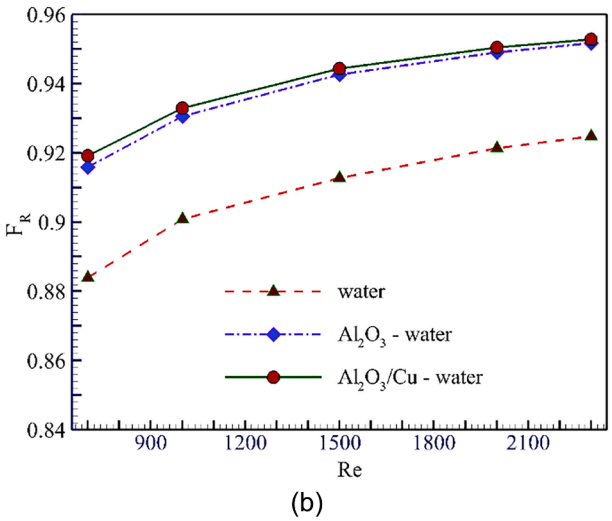

Fig. 5b. Collector heat transfer factor for various working fluids versus Re.

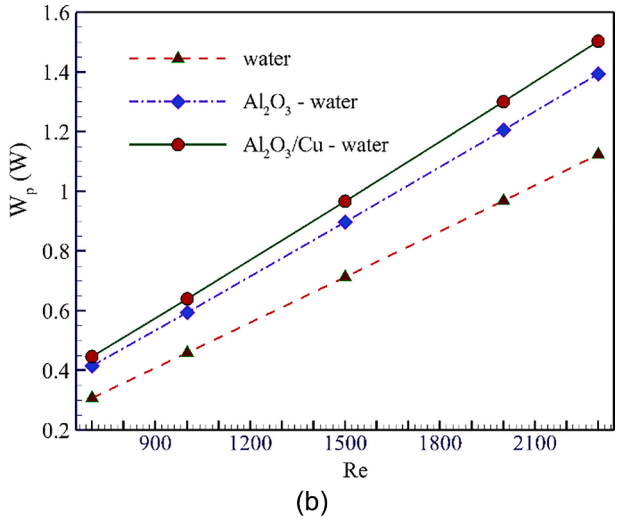

Fig. 6b. Pumping power of different working fluids in FPSC versus Re.

Table 4
F_RU_L, F_R ($\tau\alpha$) and η_{en} for FPSC for base fluid, mono nanofluid, and HYBN at Re = 2000.

Working fluid	F_RU_L	$F_R(\tau\alpha)$	η_{en}
Water	3.594	0.7191	0.6711
Aluminum oxide–water	3.573	0.7408	0.6931
Aluminum oxide/copper–water	3.571	0.7418	0.6942

from the energy point of view, the most suitable working fluid for the FPSC in the present problem is a HYBN.

Fig. 6a shows the pressure drop of HYBN, mono nanofluid, and base fluid at different Reynolds numbers. The pressure drop of aluminum oxide–water mono nanofluid is more than the base fluid and less than the HYBN. The use of nanoparticles in the base fluid causes a drop in pressure, which is one of the most important challenges in applying nanofluids in flat plate collectors. According to Fig. 6a, the pressure drop is increased with the Re because of an increase in the coefficient of friction. At Re of 2300, the increase in pressure drop of HYBN and mono nanofluid is equal to 1.3 and 1.7%, respectively, relative to water.

Evaluation of the pumping power generated in the flat plate collector circuit due to the base fluid, HYBN, and mono nanofluid is shown in Fig. 6b at various Reynolds numbers. Pumping power and pressure drop diagrams have a quantitatively similar trend. The use of nanofluids increases the pumping power and cost of the system. At Re of 2300, the pumping power of the system for water, mono nanofluid, and HYBN is 1.12, 1.4, and 1.5 W, respectively. Although the amount of pumping power due to nanofluids is more than the base fluid, their amount is negligible.

To assess the advantages of employing nanofluid, PEC is calculated. In this research, two types of PEC are used, PEC at a constant pumping power (PEC I) and at a constant pressure drop (PEC II).

Figs. 7 and 8 depict PEC I and PEC II in terms of Re, respectively. In general, HYBNs have higher PEC than base fluids and mono nanofluids. Also, increasing the Re enhances the PEC. The PEC I for HYBN and mono nanofluid at Re of 700 is 1.77 and 1.85, respectively, and at Re of 2300 is 2.77 and 2.89, respectively. The high values of PEC I are very significant for solar flat panel collectors, indicating the advantage of nanofluids. When the deposition and agglomeration of nanofluids are resolved in the future, the replacement of HYBNs with base fluids is a definite matter. According to Figs. 7 and 8, the value of PEC1 increases with increasing Reynolds number. The increase in heat transfer rate with increasing Reynolds number is the cause of this PEC1 behavior. These figures also show that the PEC1 values for hybrid nanofluids are higher than those for conventional nanofluids in similar Reynolds numbers, which indicates that the application of hybrid nanofluids is useful and effective.

The PEC for a constant pressure drop is slightly less than that for a

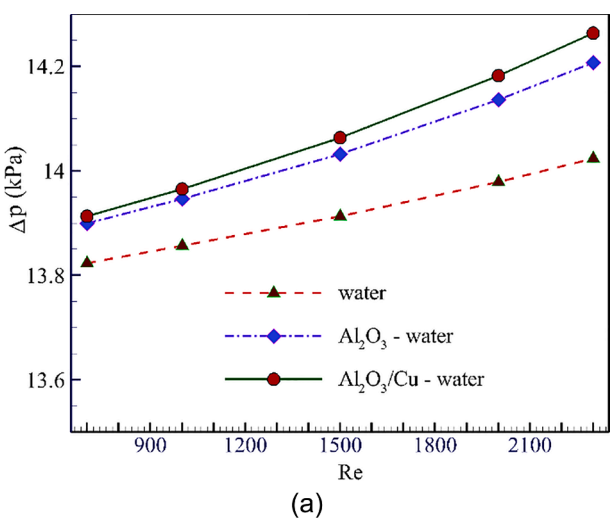

Fig. 6a. Pressure drop of the base fluid and nanofluids versus Re.

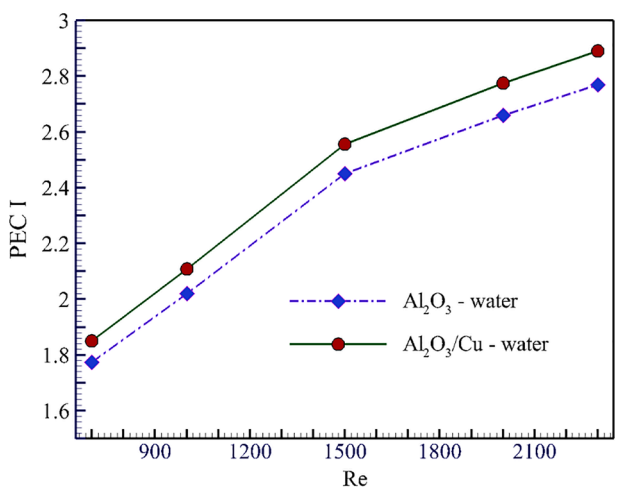

Fig. 7. PEC at a constant pumping power in terms of Re.

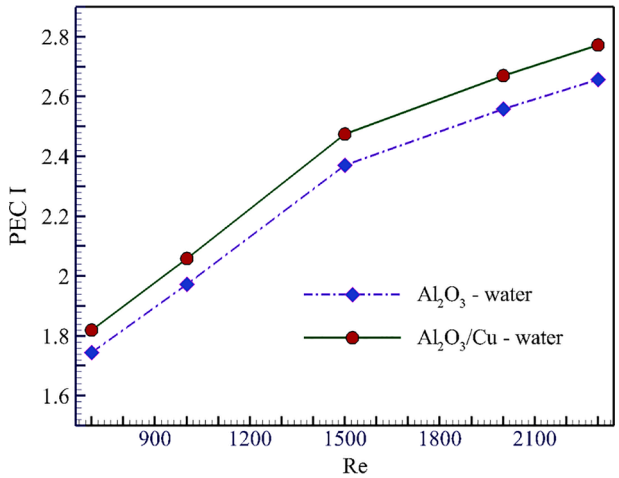

Fig. 8. PEC at a constant pressure drop in terms of Re.

constant pumping power based on Eqs. 31 and 32. Accordingly, PEC I at Re of 700 is equal to 1.65 and 1.73, and at Re of 2300 is equal to 2.66 and 2.77, respectively.

Environmental analysis

To analyze the environmental effect of the solar flat panel collector, the energy visualization approach is used. For this purpose, it is assumed that the flat plate collector consists of 10 kg of copper and 30 kg of glass [32]. The energy visualization coefficients for copper and glass are 70.6 and 15.9 MJ/kg, respectively [64], which other researchers have used for the environmental analysis of FPSC [32–34]. Based on this, the visualized energy for the FPSC is 1183 MJ for waters.

The collector surface reduction method is used to assess the amount of visualized energy of the collector when other working fluids are employed. The required collector surface is calculated as follows:

$$A_c = \frac{\dot{m} C_{pf} (T_o - T_i)}{\eta G_T} \tag{23}$$

The required collector surface is calculated for the same collector's outlet and inlet temperature for nanofluids and the base fluid and based on the amount of collector's thermal efficiency for nanofluids (Fig. 3). Thus, the reduction collector surface is 4.06 and 3.71%, respectively, when working fluid is aluminum oxide/copper–water HYBN and aluminum oxide–water mono nanofluid.

Coal, oil, and natural gas are important sources of electricity generation that also pollute the environment. Table 5 shows the production of carbon dioxide, nitrogen oxides, and sulfur oxides for these fuel sources.

The amount of visualized energy for HYBN and mono nanofluid is calculated according to the amount of surface reduction. Also, according to Table 5, the amount of different pollutants is obtained for each of the collector working fluids. Table 6 presents the amount of visualized energy as well as the amounts of production of each of the environmental pollutants, including carbon dioxide, nitrogen oxides, and sulfur oxides.

According to Table 6, the amounts of pollutants for HYBN are less than other working fluids. The rate of carbon dioxide production reduction for HYBN and mono nanofluid is 29.15 and 26.64 kg, respectively, relative to water. Also, the reduction of sulfur oxides for HYBN and mono nanofluid is 0.0149 and 0.0136 kg, respectively, relative to water. The reduction of nitrogen oxides is also 0.0255 and 0.0233 kg, respectively.

Accordingly, the most polluting working fluid is water and the cleanest one from an environmental point of view is aluminum oxide/copper–water HYBN.

Table 5
Production values of carbon dioxide, nitrogen oxides, and sulfur oxides for different fuel sources [65].

Fuel	CO_2 (kg/MJ)	NO_x (kg/MJ)	SO_x (kg/MJ)
Coal	0.274	0.00031	0.0005
oil	0.220	0	0
Natural gas	0.113	0	0.00003

Table 6
Visualized energy and amounts of pollutants for different working fluids in a FPSC.

	Water	Aluminum oxide–water	Aluminum oxide/copper–water hybrid
Visualized energy, MJ	1183	1139.11	1134.97
Carbon dioxide, kg	718.08	691.44	688.93
Sulfur oxides, kg	0.36673	0.35312	0.35184
Nitrogen oxides, kg	0.62699	0.060373	0.60153

Conclusions

In this study, different thermal and hydrodynamic parameters of a FPSC were evaluated using three various working fluids, including water, aluminum oxide/copper–water HYBN, and aluminum oxide–-water mono nanofluid. The nanoparticles' volume fraction was equal to 0.1%. After analyzing the results, it was found that:

- The thermal efficiency of the collector with HYBN is more than other working fluids. Its maximum increase in collector thermal efficiency compared to water and aluminum oxide–water mono nanofluid was 4.23 and 0.36%, respectively. Also, the maximum increment in thermal efficiency using aluminum oxide–water mono nanofluid was 3.86% compared to water.
- The amount of pumping power and pressure drop of HYBN was higher than other working fluids, but it was not significant.

The absorber plate's temperature was reduced when the nanofluids were employed instead of the base fluid. The maximum decrease in the absorber plate's temperature for the HYBN and mono nanofluid was 5.19 4.72 K, respectively, relative to water.

The PEC values at a constant pumping power and PEC at a constant pressure drop indicated that employing the HYBN instead of the mono nanofluid and base fluid was more beneficial.

- The maximum production of environmental pollutants, including carbon dioxide, nitrogen oxides, and sulfur oxides in a solar panel collector, occurred when water was applied as the working fluid, and the minimum amount of these pollutants occurred when HYBN was employed.

CRediT authorship contribution statement

Jawed Mustafa: Supervision, Writing – original draft. **Saeed Alqaed:** Validation, Writing – original draft. **Mohsen Sharifpur:** Conceptualization, Writing – review & editing.

Declaration of Competing Interest

The authors declare that they have no known competing financial interests or personal relationships that could have appeared to influence the work reported in this paper.

Acknowledgment

The authors are thankful to the Deanship of Scientific Research at Najran University for funding this work under the Research Groups Funding program grant code (NU/RG/SERC/11/15).

Appendix

Complementary correlations and equations

The amount of absorbed solar energy depends on the radiative properties of the collector, including the glass transparent coefficient (τ_c) and the absorption coefficient of the absorbent plate (α_p), as well as the total amount of impact radiation on the collector G_T and is calculated based on the following equation [49]:

$$S = 1.01\tau_c\alpha_p G_T \tag{A-1}$$

The coefficient of heat loss depends on various parameters such as emissivity (ε_p) and absorber tube's temperature, emissivity (ε_c) and the number of glass cover N, ambient temperature, air transfer heat transfer coefficient, and collector angle from the horizon (β). U_t is calculated using the following relation [50]:

$$U_t = \left(\frac{N}{\frac{C}{T_{pm}}\left(\frac{T_{pm} - T_a}{N + f}\right)^{0.33} + \frac{1}{h_w}}\right)^{-1} + \frac{\sigma\left(T_{pm}^2 + T_a^2\right)\left(T_{pm} + T_a\right)}{\frac{1}{\varepsilon_p + 0.05N\left(1 - \varepsilon_p\right)} + \frac{2N + f - 1}{\varepsilon_c} - N} \tag{A-2.1}$$

Wind heat transfer coefficient is h_w [49] where V_w is the wind velocity (m/s).

$$f = \left(1 - 0.04h_w + 0.0005h_w^2\right)(1 + 0.091N) \tag{A-2.2}$$

$$C = 365.9\left(1 - 0.00883\beta + 0.0001298\beta^2\right) \tag{A-2.3}$$

$$h_w = 2.8 + 3V_w \tag{A-2.4}$$

$$m = \sqrt{\frac{U_L}{k_p\delta_p}} \tag{A-3}$$

To calculate the base fluid's Nusselt number, the Shah equation is used [66].

$$Nu_{bf} = \begin{cases} 1.953\left(RePr\frac{D_i}{L}\right)^{\frac{1}{3}} & RePr\frac{D_i}{L} \geqslant 33.33 \\ 4.364 + 0.0722\left(RePr\frac{D_i}{L}\right) & RePr\frac{D_i}{L} < 33.33 \end{cases} \tag{A-9.1}$$

The nanofluid Nusselt number is also obtained based on the relationship of Suresh et al. [45]:

$$Nu_{nf} = 0.031(RePr)^{0.68}(1 + \phi)^{95.73} \tag{A-9.2}$$

where ϕ is the volume fraction of nanoparticles. Moreover, Pr and Re represent respectively the Prandtl and Reynolds numbers and are obtained as follows [67]:

$$Pr = \frac{\mu_f C_{pf}}{k_f} \tag{A-9.3}$$

$$Re = \frac{4\dot{m}_r}{\pi D_i \mu_f} \tag{A-9.4}$$

where $\dot{m}_r$ is the mass flow rate of each tube (riser) (kg/s).

Since the collector tubes of the FPSC are parallel, the rate of mass flow of each riser is obtained by dividing the total rate of mass flow of the collector by the number of risers, n, which is as follows [68]:

$$\dot{m}_r = \frac{\dot{m}}{n} \tag{A-9.5}$$

The output useful energy from the collector received by the working fluid is used to enhance the temperature of the fluid. Its relation to define the output fluid's temperature is defined as belows [49].

$$Q_u = \dot{m}C_{pf}(T_o - T_i) \tag{A-10.1}$$

where T_o is the working fluid's output temperature in K. The working fluid's average temperature is calculated as follows [49]:

$$T_m = T_i + \left(\frac{Q_u}{A_c U_L F_R}\right)\left(1 - \frac{F_R}{F'}\right) \tag{A-10.2}$$

h_L represents the total head loss that is the sum of the collector's major and minor head losses. h_L is defined as follows [69]:

$$h_L = \frac{8\dot{m}_r^2}{\rho_f^2 g\pi^2 D_i^4}\left(f\frac{L}{D_i} + \sum K_L\right) \tag{A-11.1}$$

Here, K_L is 0.5 for the fluid entering each riser and 1 for the fluid leaving the riser [51,69,70].
In Eq. (15), f represents the friction coefficient of the working fluid that is calculated applying the equation of Hagen-Poiseuille.

$$f_{bf} = \frac{64}{Re} \tag{A-11.2}$$

The coefficient of nanofluid friction is obtained employing the relation of Suresh et al. [45].

$$f_{nf} = \frac{26.44}{Re^{0.8737}}(1+\phi)^{156.23} \tag{A-11.3}$$

The base fluid's thermophysical properties are assumed to be a function of temperature and are calculated at the fluid's average temperature. Water density is obtained as follows [55]:

$$\rho_{bf} = -3\times 10^{-3}T_m^2 + 1.505T_m + 816.781 \tag{A-15.1}$$

The specific heat of water is calculated as follows [55]:

$$C_{pbf} = -4.63\times 10^{-5}\times T_m^3 + 0.0552\times T_m^2 - 20.86\times T_m + 6719.637 \tag{A-15.2}$$

The thermal conductivity of water is calculated using the relation of De Castro et al. [56]:

$$k_{bf} = 0.6067\left[-1.26523 + 3.70483\left(\frac{T_m}{298.15}\right) - 1.43955\left(\frac{T_m}{298.15}\right)^2\right] \tag{A-15.3}$$

The dynamic viscosity of water is calculated using the following equation [71]:

$$\mu_{bf} = 2.414\times 10^{-5}\times 10^{\frac{247.8}{T_m-140}} \tag{A-15.4}$$

The density and specific heat and density of the nanocomposite and nanofluid are determined based on the (22-a) to (22-d) equations [61,62].

$$\rho_{np} = \frac{\rho_{np1}\phi_1 + \rho_{np2}\phi_2}{\phi} \tag{A-15.5}$$

$$C_{pnp} = \frac{C_{pnp1}\rho_{np1}\phi_1 + C_{pnp2}\rho_{np2}\phi_2}{\rho_{np}\phi} \tag{A-15.6}$$

$$\rho_{nf} = (1-\phi)\rho_{bf} + \phi\rho_{np} \tag{A-15.7}$$

$$C_{pnf} = \frac{(1-\phi)\rho_{bf}C_{pbf} + \phi\rho_{np}C_{pnp}}{\rho_{nf}} \tag{A-15.8}$$

References

[1] Syam Sundar L, Mesfin S, Tefera Sintie Y, Punnaiah V, Chamkha AJ, Sousa A. A review on the use of hybrid nanofluid in a solar flat plate and parabolic trough collectors and its enhanced collector thermal efficiency. J Nanofluids 2021;10:147–71.
[2] Fan S, Wang Y, Cao S, Zhao B, Sun T, Liu P. A deep residual neural network identification method for uneven dust accumulation on photovoltaic (PV) panels. Energy 2022;239:122302.
[3] Cai T, Dong M, Liu H, Nojavan S. Integration of hydrogen storage system and wind generation in power systems under demand response program: A novel p-robust stochastic programming. Int J Hydrogen Energy 2022;47(1):443–58.
[4] Chen X, Quan Q, Zhang K, Wei J. Spatiotemporal characteristics and attribution of dry/wet conditions in the Weihe River Basin within a typical monsoon transition zone of East Asia over the recent 547 years. Environ Modell Software 2021;143:105116.
[5] Schwalm CR, Huntinzger DN, Michalak AM, Fisher JB, Kimball JS, Mueller B, et al. Sensitivity of inferred climate model skill to evaluation decisions: a case study using CMIP5 evapotranspiration. Environ Res Lett 2013;8:024028.
[6] Zhu D, Wang B, Ma H, Wang H. Evaluating the vulnerability of integrated electricity-heat-gas systems based on the high-dimensional random matrix theory. CSEE J Power Energy Syst 2019;6:878–89.
[7] Zhang X, Tang Y, Zhang F, Lee C-S. A novel aluminum–graphite dual-ion battery. Adv Energy Mater 2016;6(11):1502588.
[8] Li X, Gui De, Zhao Z, Li X, Wu X, Hua Y, et al. Operation optimization of electrical-heating integrated energy system based on concentrating solar power plant hybridized with combined heat and power plant. J Cleaner Prod 2021;289:125712.
[9] Fan S, Wang Yu, Cao S, Sun T, Liu P. A novel method for analyzing the effect of dust accumulation on energy efficiency loss in photovoltaic (PV) system. Energy 2021;234:121112.
[10] Alawi OA, Kamar HM, Mallah AR, Mohammed HA, Sabrudin MAS, Newaz KM, et al. Experimental and theoretical analysis of energy efficiency in a flat plate solar collector using monolayer graphene nanofluids. Sustainability 2021;13:5416.
[13] Al-Rashed AAAA, Ranjbarzadeh R, Aghakhani S, Soltanimehr M, Afrand M, Nguyen TK. Entropy generation of boehmite alumina nanofluid flow through a minichannel heat exchanger considering nanoparticle shape effect. Physica A 2019;521:724–36.
[14] Kazemi I, Sefid M, Afrand M. A novel comparative experimental study on rheological behavior of mono & hybrid nanofluids concerned graphene and silica nano-powders: Characterization, stability and viscosity measurements. Powder Technol 2020;366:216–29.
[15] Hemmat Esfe M, Reiszadeh M, Esfandeh S, Afrand M. Optimization of MWCNTs (10%) – Al2O3 (90%)/5W50 nanofluid viscosity using experimental data and artificial neural network. Physica A 2018;512:731–44.
[16] Yan S-R, Golzar A, Sharifpur M, Meyer JP, Liu D-H, Afrand M. Effect of U-shaped absorber tube on thermal-hydraulic performance and efficiency of two-fluid parabolic solar collector containing two-phase hybrid non-Newtonian nanofluids. Int J Mech Sci 2020;185:105832.
[17] Pordanjani AH, Aghakhani S, Afrand M, Sharifpur M, Meyer JP, Xu H, et al. Nanofluids: Physical phenomena, applications in thermal systems and the environment effects- a critical review. J Cleaner Prod 2021;320:128573.
[18] Sheikholeslami M, Farshad SA, Ebrahimpour Z, Said Z. Recent progress on flat plate solar collectors and photovoltaic systems in the presence of nanofluid: a review. J Cleaner Prod 2021;293:126119.
[19] Aybar HŞ, Sharifpur M, Azizian MR, Mehrabi M, Meyer JP. A review of thermal conductivity models for nanofluids. Heat Transfer Eng 2015;36:1085–110.
[20] Li X, Zeng G, Lei X. The stability, optical properties and solar-thermal conversion performance of SiC-MWCNTs hybrid nanofluids for the direct absorption solar collector (DASC) application. Sol Energy Mater Sol Cells 2020;206:110323.
[21] Hemmat Esfe M, Abbasian Arani AA, Esfandeh S, Afrand M. Proposing new hybrid nano-engine oil for lubrication of internal combustion engines: preventing cold start engine damages and saving energy. Energy 2019;170:228–38.

[22] Al-Yasiri Q, Szabó M, Arıcı M. Single and hybrid nanofluids to enhance performance of flat plate solar collectors: application and obstacles. Periodica Polytechnica Mech Eng 2021;65:86–102.
[23] Farajzadeh E, Movahed S, Hosseini R. Experimental and numerical investigations on the effect of Al2O3/TiO2H2O nanofluids on thermal efficiency of the flat plate solar collector. Renewable Energy 2018;118:122–30.
[24] Verma SK, Tiwari AK, Tiwari S, Chauhan DS. Performance analysis of hybrid nanofluids in flat plate solar collector as an advanced working fluid. Sol Energy 2018;167:231–41.
[25] Hussein OA, Habib K, Muhsan AS, Saidur R, Alawi OA, Ibrahim TK. Thermal performance enhancement of a flat plate solar collector using hybrid nanofluid. Sol Energy 2020;204:208–22.
[26] Okonkwo EC, Wole-Osho I, Kavaz D, Abid M, Al-Ansari T. Thermodynamic evaluation and optimization of a flat plate collector operating with alumina and iron mono and hybrid nanofluids. Sustainable Energy Technol Assess 2020;37:100636.
[27] Ja RB, Kumar K. Thermodynamic analysis of hybrid nanofluid based solar flat plate collector. World J Eng 2018.
[28] Wole-Osho I, Okonkwo EC, Kavaz D, Abbasoğlu S. Energy, exergy, and economic investigation of the effect of nanoparticle mixture ratios on the thermal performance of flat plate collectors using Al 2 O 3–ZnO hybrid nanofluid. J Energy Eng 2021;147:04020083.
[29] Sundar LS, Mesfin S, Said Z, Singh MK, Punnaiah V, Sousa ACM. Energy, economic, environmental and heat transfer analysis of a solar flat-plate collector with pH-treated Fe 3 O 4/water nanofluid. Int J Energy Clean Environ 2021;22(6):55–98.
[30] Tahat MS, Benim AC, Experimental analysis on thermophysical properties of Al2O3/CuO hybrid nano fluid with its effects on flat plate solar collector, in: Defect and diffusion forum, Vol. 374, Trans Tech Publ, 2017, pp. 148-156.
[31] Syam Sundar L, Misganaw A, Singh MK, Sousa A, Ali HM. Efficiency analysis of thermosyphon solar flat plate collector with low mass concentrations of ND–Co3O4 hybrid nanofluids: an experimental study. J Therm Anal Calorim 2021;143:959–72.
[32] Faizal M, Saidur R, Mekhilef S, Alim MA. Energy, economic and environmental analysis of metal oxides nanofluid for flat-plate solar collector. Energy Convers Manage 2013;76:162–8.
[33] Michael Joseph Stalin P, Arjunan T, Matheswaran M, Dolli H, Sadanandam N, Energy, economic and environmental investigation of a flat plate solar collector with CeO2/water nanofluid, J Thermal Anal Calorimetry, 139 (2020) 3219-3233.
[34] Faizal M, Saidur R, Mekhilef S, Hepbasli A, Mahbubul I. Energy, economic, and environmental analysis of a flat-plate solar collector operated with SiO2 nanofluid. Clean Technol Environ Policy 2015;17:1457–73.
[35] Jamal-Abad MT, Zamzamian A, Imani E, Mansouri M. Experimental study of the performance of a flat-plate collector using Cu–water nanofluid. J Thermophys Heat Transfer 2013;27:756–60.
[36] Xiong Q, Hajjar A, Alshuraiaan B, Izadi M, Altnji S, Shehzad SA. State-of-the-art review of nanofluids in solar collectors: a review based on the type of the dispersed nanoparticles. J Cleaner Prod 2021;310:127528.
[37] Alqaed S, Mustafa J, Sharifpur M, Cheraghian G. Using nanoparticles in solar collector to enhance solar-assisted hot process stream usefulness. Sustainable Energy Technol Assess 2022;52:101992.
[38] Alqaed S, Almehmadi FA, Mustafa J, Husain S, Cheraghian G. Effect of nano phase change materials on the cooling process of a triangular lithium battery pack. J Storage Mater 2022;51:104326.
[39] Mustafa J, Almehmadi FA, Alqaed S. A novel study to examine dependency of indoor temperature and PCM to reduce energy consumption in buildings. J Build Eng 2022;51:104249.
[40] Alqaed S, Mustafa J, Almehmadi FA. The effect of using phase change materials in a solar wall on the number of times of air conditioning per hour during day and night in different thicknesses of the solar wall. J Build Eng 2022;51:104227.
[41] Mustafa J, Alqaed S, Sharifpur M. Incorporating nano-scale material in solar system to reduce domestic hot water energy demand. Sustainable Energy Technol Assess 2022;49:101735.
[42] Suresh S, Venkitaraj K, Hameed MS, Sarangan J. Turbulent heat transfer and pressure drop characteristics of dilute water based Al2O3–Cu hybrid nanofluids. J Nanosci Nanotechnol 2014;14:2563–72.
[43] Shahul Hameed M, Suresh S, Singh RK. Comparative study of heat transfer and friction characteristics of water-based Alumina–copper and Alumina–CNT hybrid nanofluids in laminar flow through pipes. J Therm Anal Calorim 2019;136:243–53.
[44] Suresh S, Venkitaraj KP, Selvakumar P, Chandrasekar M. Synthesis of Al2O3–Cu/water hybrid nanofluids using two step method and its thermo physical properties. Colloids Surf, A 2011;388(1-3):41–8.
[45] Suresh S, Venkitaraj K, Selvakumar P, Chandrasekar M. Effect of Al2O3–Cu/water hybrid nanofluid in heat transfer. Exp Therm Fluid Sci 2012;38:54–60.
[46] Amirahmad A, Maglad AM, Mustafa J, Cheraghian G. Loading PCM into buildings envelope to decrease heat gain-Performing transient thermal analysis on nanofluid filled solar system. Front Energy Res 2021;9:727011.
[47] Mustafa J, Alqaed S, Kalbasi R. Challenging of using CuO nanoparticles in a flat plate solar collector-Energy saving in a solar-assisted hot process stream. J Taiwan Inst Chem Eng 2021;124:258–65.
[48] Mansour MK. Thermal analysis of novel minichannel-based solar flat-plate collector. Energy 2013;60:333–43.
[49] Duffie JA, Beckman WA, Blair N. Solar engineering of thermal processes, photovoltaics and wind. John Wiley & Sons; 2020.
[50] Kalogirou SA. Solar energy engineering: processes and systems. Academic press; 2013.
[51] Mahian O, Kianifar A, Sahin AZ, Wongwises S. Entropy generation during Al2O3/water nanofluid flow in a solar collector: Effects of tube roughness, nanoparticle size, and different thermophysical models. Int J Heat Mass Transf 2014;78:64–75.
[52] Vahidinia F, Khorasanizadeh H, Aghaei A. Comparative energy, exergy and CO2 emission evaluations of a LS-2 parabolic trough solar collector using Al2O3/SiO2-Syltherm 800 hybrid nanofluid. Energy Convers Manage 2021;245:114596.
[53] Arani AA, Amani J. Experimental study on the effect of TiO2–water nanofluid on heat transfer and pressure drop. Exp Therm Fluid Sci 2012;42:107–15.
[54] Bellos E, Tzivanidis C, Tsimpoukis D. Multi-criteria evaluation of parabolic trough collector with internally finned absorbers. Appl Energy 2017;205:540–61.
[55] Edalatpour M, Solano JP. Thermal-hydraulic characteristics and exergy performance in tube-on-sheet flat plate solar collectors: effects of nanofluids and mixed convection. Int J Therm Sci 2017;118:397–409.
[56] Nieto de Castro CA, Li SFY, Nagashima A, Trengove RD, Wakeham WA. Standard reference data for the thermal conductivity of liquids. J Phys Chem Ref Data 1986;15(3):1073–86.
[57] Mehryan SAM, Izadpanahi E, Ghalambaz M, Chamkha AJ. Mixed convection flow caused by an oscillating cylinder in a square cavity filled with Cu–Al2O3/water hybrid nanofluid. J Therm Anal Calorim 2019;137(3):965–82.
[58] Mehryan SAM, Kashkooli FM, Ghalambaz M, Chamkha AJ. Free convection of hybrid Al2O3-Cu water nanofluid in a differentially heated porous cavity. Adv Powder Technol 2017;28(9):2295–305.
[59] Rajesh V, Srilatha M, Chamkha AJ. Hydromagnetic effects on hybrid nanofluid (Cu–Al2O3/Water) flow with convective heat transfer due to a stretching sheet. J Nanofluids 2020;9(4):293–301.
[60] Jamaludin A, Naganthran K, Nazar R, Pop I. MHD mixed convection stagnation-point flow of Cu-Al2O3/water hybrid nanofluid over a permeable stretching/shrinking surface with heat source/sink. Eur J Mech-B/Fluids 2020;84:71–80.
[61] Khan MS, Abid M, Bashir MA, Amber KP, Khanmohammadi S, Yan M. Thermodynamic and exergoeconomic analysis of a novel solar-assisted multigenerational system utilizing high temperature phase change material and hybrid nanofluid. Energy Convers Manage 2021;236:113948.
[62] Abid M, Khan MS, Ratlamwala TAH, Malik MN, Ali HM, Cheok Q. Thermodynamic analysis and comparison of different absorption cycles driven by evacuated tube solar collector utilizing hybrid nanofluids. Energy Convers Manage 2021;246:114673.
[63] Jafarkazemi F, Ahmadifard E. Energetic and exergetic evaluation of flat plate solar collectors. Renewable Energy 2013;56:55–63.
[64] Baird G, Alcorn A, Haslam P. The energy embodied in building materials-updated New Zealand coefficients and their significance. Trans Inst Professional Eng New Zealand: Civil Eng Section 1997;24:46–54.
[65] Mashhadian A, Heyhat MM, Mahian O. Improving environmental performance of a direct absorption parabolic trough collector by using hybrid nanofluids. Energy Convers Manage 2021;244:114450.
[66] Shah R, Thermal entry length solutions for the circular tube and parallel plates, in: Proceedings of 3rd national heat and mass transfer conference, Vol. 1, Indian Institute of Technology Bombay, 1975, pp. 11-75.
[67] Bergman TL, Bergman TL, Incropera FP, Dewitt DP, Lavine AS. Fundamentals of heat and mass transfer. John Wiley & Sons; 2011.
[68] Vahidinia F, Khorasanizadeh H. Development of new algebraic derivations to analyze minichannel solar flat plate collectors with small and large size minichannels and performance evaluation study. Energy 2021;228:120640.
[69] Mahian O, Kianifar A, Sahin AZ, Wongwises S. Performance analysis of a minichannel-based solar collector using different nanofluids. Energy Convers Manage 2014;88:129–38.
[70] Mahian O, Kianifar A, Heris SZ, Wongwises S. First and second laws analysis of a minichannel-based solar collector using boehmite alumina nanofluids: effects of nanoparticle shape and tube materials. Int J Heat Mass Transf 2014;78:1166–76.
[71] Khanafer K, Vafai K. A critical synthesis of thermophysical characteristics of nanofluids. Int J Heat Mass Transf 2011;54:4410–28.
[72] Mustafa J, Alqaed S, Sharifpur M, Husain S. The effect of using multichannel twisted tape and nanofluid on the absorber tube's heat transfer and the efficiency of a linear parabolic solar collector. Sustainable Energy Technologies and Assessments 2022;52:102329.
[73] Mustafa J. Numerical investigation of the effect of inlet dimensions air duct and distance of battery packs for thermal management of three lithium-ion battery packs. Journal of Energy Storage 2022;48:103959.
[74] Mustafa J, Alqaed S, Siddiqui MA. Thermally Driven Flow of Water in Partially Heated Tall Vertical Concentric Annulus. Entropy 2020;22(10):1189.
[75] Mustafa J, Alqaed S, Sharifpur M. Loading phase change material in a concrete based wall to enhance concrete thermal properties. Journal of Building Engineering 2022;56:104765.
[76] Mustafa J, Siddiqui MA, Anwer SF. Experimental and Numerical Analysis of Heat Transfer in a Tall Vertical Concentric Annular Thermo-siphon at Constant heat Flux Condition. Heat Transfer Engineering 2019;40(11):896–913.